Title
MAJOR OXIDE, MINOR OXIDE, AND TRACE ELEMENT ANALYSIS OF ANDESITE AND DACITE ARTIFACTS FROM 5LA1211 AND 5LA1416, SOUTHERN COLORADO

Author
Shackley, M. Steven

Publication Date
2017-09-01

GEOARCHAEOLOGICAL XRF LAB
A Green Solar Facility

GEOARCHAEOLOGICAL X-RAY FLUORESCENCE SPECTROMETRY LABORATORY
8100 Wyoming Blvd., Ste M4-158 Albuquerque, NM 87113 USA

MAJOR OXIDE, MINOR OXIDE, AND TRACE ELEMENT ANALYSIS OF ANDESITE AND DACITE ARTIFACTS FROM 5LA1211 AND 5LA1416, SOUTHERN COLORADO

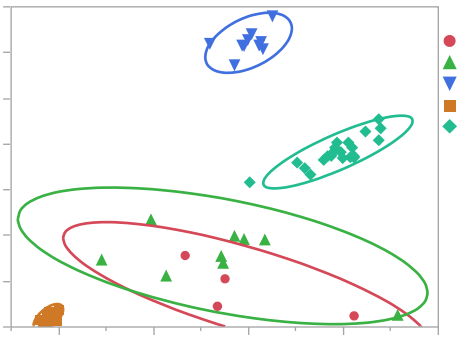

by

M. Steven Shackley, Ph.D., Director
Geoarchaeological XRF Laboratory
Albuquerque, New Mexico

Report Prepared for

Sara Cullen
Department of Anthropology
University of Colorado
Boulder, Colorado

1 September 2017

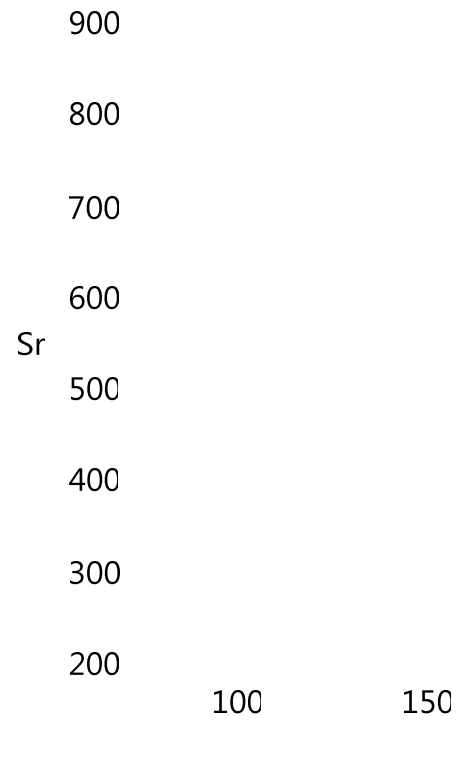

INTRODUCTION

The analysis here of volcanic rock artifacts indicates that all the samples were produced from intermediate andesite and dacite volcanic rocks. While the rocks are certainly intermediate volcanic rocks, the dacite artifacts do not match any known archaeological dacite source from the Taos Plateau Volcanic Field such as San Antonio Mountain or Newman Dome approximately 135 km southwest of Trinidad, Colorado (Shackley 2011a).

LABORATORY SAMPLING, ANALYSIS AND INSTRUMENTATION

All samples are analyzed whole. The results presented here are quantitative in that they are derived from "filtered" intensity values ratioed to the appropriate x-ray continuum regions through a least squares fitting formula rather than plotting the proportions of the net intensities in a ternary system (McCarthy and Schamber 1981; Schamber 1977). Or more essentially, these data through the analysis of international rock standards, allow for inter-instrument comparison with a predictable degree of certainty (Hampel 1984; Shackley 2011b).

All analyses for this study were conducted on a ThermoScientific *Quant'X* EDXRF spectrometer, located at the Geoarchaeological XRF Laboratory, Albuquerque, New Mexico. It is equipped with a thermoelectrically Peltier cooled solid-state Si(Li) X-ray detector, with a 50 kV, 50 W, ultra-high-flux end window bremsstrahlung, Rh target X-ray tube and a 76 μm (3 mil) beryllium (Be) window (air cooled), that runs on a power supply operating from 4-50 kV/0.02-1.0 mA at 0.02 increments. The spectrometer is equipped with a 200 l min^{-1} Edwards vacuum pump, allowing for the analysis of lower-atomic-weight elements between sodium (Na) and titanium (Ti). Data acquisition is accomplished with a pulse processor and an analogue-to-digital converter. Elemental composition is identified with digital filter background removal, least squares empirical peak deconvolution, gross peak intensities and net peak intensities above background.

Trace Element Analysis

In the analysis for mid Zb/Zc condition elements Ti-Nb, Pb, Th, the x-ray tube is operated at 30 kV, using a 0.05 mm (medium) Pd primary beam filter in an air path at 100 seconds livetime to generate x-ray intensity Ka-line data for elements titanium (Ti), manganese (Mn), iron (as $Fe_2O_3^T$), cobalt (Co), nickel (Ni), copper, (Cu), zinc, (Zn), gallium (Ga), rubidium (Rb), strontium (Sr), yttrium (Y), zirconium (Zr), niobium (Nb), lead (Pb), and thorium (Th). Not all these elements are reported since their values in many volcanic rocks are very low. Trace element intensities were converted to concentration estimates by employing a linear calibration line ratioed to the Compton scatter established for each element from the analysis of international rock standards certified by the National Institute of Standards and Technology (NIST), the US. Geological Survey (USGS), Canadian Centre for Mineral and Energy Technology, and the Centre de Recherches Pétrographiques et Géochimiques in France (Govindaraju 1994). Line fitting is linear (XML) for all elements. When barium (Ba) is analyzed in the High Zb condition, the Rh tube is operated at 50 kV and up to 1.0 mA, ratioed to the bremsstrahlung region (see Davis 2011; Shackley 2011b). Further details concerning the petrological choice of these elements in Southwest volcanic rocks is available in Shackley (1988, 1995, 2005; also Mahood and Stimac 1991; and Hughes and Smith 1993). Nineteen specific pressed powder standards are used for the best fit regression calibration for elements Ti-Nb, Pb, Th, and Ba, and include G-2 (basalt), AGV-2 (andesite), GSP-2 (granodiorite), SY-2 (syenite), BHVO-2 (hawaiite), STM-1 (syenite), QLO-1 (quartz latite), RGM-1 (obsidian), W-2 (diabase), BIR-1 (basalt), SDC-1 (mica schist), TLM-1 (tonalite), SCO-1 (shale), NOD-A-1 and NOD-P-1 (manganese) all US Geological Survey standards, NIST-278 (obsidian), U.S. National Institute of Standards and Technology, BE-N (basalt) from the Centre de Recherches Pétrographiques et

Géochimiques in France, and JR-1 and JR-2 (obsidian) from the Geological Survey of Japan (Govindaraju 1994).

Major and Minor Oxide Analysis

Analysis of the major oxides of Na, Mg, Al, Si, K, Ca, Ti, V, Mn, Fe, and the trace element Cl is performed under the multiple conditions elucidated below. This fundamental parameter analysis (theoretical with standards), while not as accurate as destructive analyses (pressed powder and fusion disks) is usually within a few percent of actual, based on the analysis of USGS AGV-1 andesite standard (see also Shackley 2011b). The fundamental parameters (theoretical) method is run under conditions commensurate with the elements of interest and calibrated with 11 USGS standards (RGM-1, rhyolite; AGV-2, andesite; BHVO-1, hawaiite; BIR-1, basalt; G-2, granite; GSP-2, granodiorite; BCR-2, basalt; W-2, diabase; QLO-1, quartz latite; STM-1, syenite), and one Japanese Geological Survey rhyolite standard (JR-1). See Lundblad et al. (2011) for another set of conditions and methods for oxide analyses.

Conditions Of Fundamental Parameter Analysis[1]:

Low Za (Na, Mg, Al, Si, P)

Voltage	6 kV	Current	Auto[2]
Livetime	100 seconds	Counts Limit	0
Filter	No Filter	Atmosphere	Vacuum
Maximum Energy	10 keV	Count Rate	Low

Low Zb (S, Cl, K, Ca)

Voltage	8 kV	Current	Auto
Livetime	100 seconds	Counts Limit	0
Filter	Cellulose (0.06 mm)	Atmosphere	Vacuum
Maximum Energy	10 keV	Count Rate	Low

Mid Zb (K, Ca, Ti, V, Cr, Mn, Fe)

Voltage	32 kV	Current	Auto
Livetime	100 seconds	Counts Limit	0
Filter	Pd (0.06 mm)	Atmosphere	Vacuum
Maximum Energy	40 keV	Count Rate	Medium

High Zb (Sn, Sb, Ba, Ag, Cd)

Voltage	50 kV	Current	Auto
Livetime	100 seconds	Counts Limit	0
Filter	Cu (0.559 mm)	Atmosphere	Vacuum
Maximum Energy	40 keV	Count Rate	High

[1] Multiple conditions designed to ameliorate peak overlap identified with digital filter background removal, least squares empirical peak deconvolution, gross peak intensities and net peak intensities above background.

[2] Current is set automatically based on the mass absorption coefficient.

Statistical and Graphical Source Assignment.

The data from the WinTrace^{TM} software were translated directly into Excel for Windows software for manipulation and on into JMP 12.0.1 for Windows for statistical analyses. In order to evaluate these quantitative determinations, machine data were compared to measurements of known standards during each run. AGV-1 a USGS andesite standard was analyzed during each sample run of ≤ 20 samples for the samples to insure machine calibration (Table 1).

DISCUSSION OF RESULTS

The major and minor oxide data were examined first to determine the potential variability in rock type, in this case andesite or dacite (Table 1 and Figure 1). The assemblage is about evenly divided between andesite and dacite, two compositionally related intermediate volcanic rocks. Andesite and dacite shields (San Antonio Mountain), stratovolcanoes and domes (Newman Dome) are common in the Taos Plateau Volcanic Field, so it is not surprising that

these are the dominant rock types used to produce artifacts at these sites (Boyer 2010; Lipman 1979; Newman and Nielson 1987; Shackley 2011a).

The trace element data were then used to determine whether the artifacts produced from dacite were procured from any of the known archaeological dacite sources in northern New Mexico (Table 1 and Figure 2). None of the artifacts were produced from any of the three known dacite sources in the Taos Plateau or Cerros del Rio volcanic fields (see Figure 2). Original cortex is not common on these artifacts, and given that they are not produced from either of the known dacite sources on the Taos Plateau (San Antonio Mountain is about 135 km southeast), these artifacts were either originally reduced at the sources, and/or are not nearby. Since there are no compositional data from any other andesite or dacite sources either on the Taos Plateau, or elsewhere, we cannot say much more.

REFERENCES CITED

Boyer, J.L., 2010, Identifying volcanic material sources in the Taos Valley. In: Brown, E.J., Armstrong, K., Brugge, D.M., Condie, C.J. (Eds.), Threads, Tints, and Edification: Papers in Honor of Glenna Dean. Papers of the Archaeological Society of New Mexico, Albuquerque, pp. 21-32.

Davis, M.K., T.L. Jackson, M.S. Shackley, T. Teague, and J. Hampel, 2011, Factors Affecting the Energy-Dispersive X-Ray Fluorescence (EDXRF) Analysis of Archaeological Obsidian. In *X-Ray Fluorescence Spectrometry (XRF) in Geoarchaeology*, edited by M.S. Shackley, pp. 45-64. Springer, New York.

Govindaraju, K., 1994, 1994 Compilation of Working Values and Sample Description for 383 Geostandards. *Geostandards Newsletter* 18 (special issue).

Hampel, Joachim H., 1984, Technical Considerations in X-ray Fluorescence Analysis of Obsidian. In *Obsidian Studies in the Great Basin*, edited by R.E. Hughes, pp. 21-25. Contributions of the University of California Archaeological Research Facility 45. Berkeley.

Hildreth, W., 1981, Gradients in Silicic Magma Chambers: Implications for Lithospheric Magmatism. *Journal of Geophysical Research* 86:10153-10192.

Hughes, Richard E., and Robert L. Smith, 1993, Archaeology, Geology, and Geochemistry in Obsidian Provenance Studies. *In Scale on Archaeological and Geoscientific Perspectives*, edited by J.K. Stein and A.R. Linse, pp. 79-91. Geological Society of America Special Paper 283.

Le Maitre, R.; Bateman, P.; Dudek, A.; Keller, J.; Lameyre, J.; Le Bas, M.; Sabine, P.; Schmid, R.; Sorensen, H.; Streckeisen, A.; Woolley, A.; Zanettin, B. 1989, A classification of igneous rocks and glossary of terms: recommendations of the International Union of Geological Sciences Subcommission on the Systematics of ingeous rocks (Le Maitre, R.W.; editor). Blackwell, 193 p. Oxford.

Lundblad, S.P., P.R. Mills, A. Drake-Raue, and S.K. Kikiloi, 2011, Non-destructive EDXRF analyses of archaeological basalts. In *In M.S. Shackley (Ed.) X-Ray Fluorescence Spectrometry (XRF) in Geoarchaeology*, pp. 65-80. Springer Publishing, New York.

Mahood, Gail A., and James A. Stimac, 1990, Trace-Element Partitioning in Pantellerites and Trachytes. *Geochemica et Cosmochimica Acta* 54:2257-2276.

McCarthy, J.J., and F.H. Schamber, 1981, Least-Squares Fit with Digital Filter: A Status Report. In *Energy Dispersive X-ray Spectrometry*, edited by K.F.J. Heinrich, D.E. Newbury, R.L. Myklebust, and C.E. Fiori, pp. 273-296. National Bureau of Standards Special Publication 604, Washington, D.C.

Newman, J.R., Nielsen, R.L., 1987, Initial notes on the x-ray fluorescence characterization of the rhyodacite sources of the Taos Plateau, New Mexico. *Archaeometry* 29: 262-275.

Schamber, F.H., 1977, A Modification of the Linear Least-Squares Fitting Method which Provides Continuum Suppression. In *X-ray Fluorescence Analysis of Environmental Samples*, edited by T.G. Dzubay, pp. 241-257. Ann Arbor Science Publishers.

Shackley, M.S., 1988, Sources of archaeological obsidian in the southwest: an archaeological, petrological, and geochemical study. *American Antiquity* 53:752-772.

Shackley, M. S.,1995, Sources of archaeological obsidian in the greater american southwest: an update and quantitative analysis. *American Antiquity* 60(3):531-551.

Shackley, M.S., 2005, *Obsidian: Geology and Archaeology in the North American Southwest*. University of Arizona Press, Tucson.

Shackley, M.S., 2011a, Sources of archaeological dacite in northern New Mexico. *Journal of Archaeological Science* 38:1001-1007.

Shackley, M.S., 2011b, An Introduction to X-Ray Fluorescence (XRF) Analysis in Archaeology. In *X-Ray Fluorescence Spectrometry (XRF) in Geoarchaeology*, M.S. Shackley (Ed.), pp. 7-44. Springer, New York.

Table 1. Major, minor oxides and trace element concentrations for the artifacts.

Sample	Site	Na2O	MgO	Al2O3	SiO2	Cl	K2O	CaO	TiO2	V2O5	MnO	Fe2O3	Rock Type
		%	%	%	%	ppm	%	%	%	%	%	%	
1	5LA1211	1.185	1.956	26.112	62.127	567	2.141	0.617	1.322	0.063	0.01	4.152	andesite
2	5LA1211	1.683	3.561	17.97	61.926	543	2.855	2.471	0.876	0.057	0.045	8.227	andesite
3	5LA1211	1.116	1.584	28.175	60.426	640	2.179	0.549	1.312	0.082	0.011	4.248	andesite
4	5LA1211	1.053	1.901	27.588	59.343	89	2.285	0.956	1.369	0.072	0.014	5.149	andesite
5	5LA1211	1.263	1.884	25.633	60.88	0	3.235	0.48	1.105	0.063	0.021	5.114	andesite
6	5LA1211	1.79	0.853	21.371	66.872	1739	3.371	0.376	0.983	0.064	0.012	3.843	dacite
7	5LA1211	0.995	0.65	25.258	62.88	491	3.055	0.997	1.307	0.088	0.014	4.409	andesite
8	5LA1211	1.46	1.872	21.951	64.815	0	3.282	0.56	0.996	0.059	0.049	4.696	dacite
9	5LA1211	1.111	1.724	26.6	62.111	106	2.069	0.505	1.105	0.074	0.014	4.462	andesite
10	5LA1211	1.241	1.365	27.817	59.001	463	2.564	0.515	1.289	0.086	0.014	5.758	andesite
11	5LA1211	1.221	1.303	22.535	67.542	263	2.057	0.514	1.267	0.047	0.011	3.275	dacite
12	5LA1211	1.232	1.384	21.832	68.517	0	2.14	0.544	0.935	0.058	0.011	3.093	dacite
13	5LA1211	0.998	1.429	26.427	62.362	531	1.997	0.497	1.254	0.061	0.01	4.679	andesite
14	5LA1211	1.303	1.675	28.453	58.861	253	2.184	0.584	1.148	0.071	0.015	5.403	andesite
15	5LA1211	1.098	1.415	26.658	61.759	0	2.423	0.527	1.278	0.081	0.012	4.482	andesite
16	5LA1416	1.221	1.6	27.721	58.459	289	2.398	0.785	1.34	0.078	0.014	6.057	andesite
17	5LA1416	0.961	1.069	25.888	62.356	101	2.491	0.471	1.096	0.051	0.015	5.342	andesite
18	5LA1416	1.176	0.265	0.894	95.104	482	0.124	0.125	1.539	0.034	0.004	0.576	andesite
19	5LA1416	1.332	0.69	20.891	66.114	0	2.435	0.514	0.942	0.054	0.013	6.782	dacite
20	5LA1416	1.839	0.863	18.36	69.713	512	1.883	0.513	0.822	0.025	0.024	5.697	dacite
21	5LA1416	2.839	2.248	15.683	64.128	0	3.702	4.212	0.89	0.049	0.128	5.745	dacite
22	5LA1416	1.276	1.144	26.564	63.168	195	2.444	0.714	0.893	0.083	0.011	3.434	dacite
23	5LA1416	1.097	1.128	28.427	60.949	508	1.863	0.496	1.062	0.051	0.01	4.632	andesite
24	5LA1416	0.947	1.23	27.568	61.729	0	1.891	0.422	1.211	0.07	0.013	4.703	andesite
25	5LA1416	1.049	1.146	26.448	60.026	206	2.167	0.74	1.306	0.076	0.042	6.671	andesite
26	5LA1416	1.709	0.728	19.929	66.963	0	2.213	0.53	0.911	0.055	0.013	6.726	dacite
27	5LA1416	1.277	0.981	19.584	69.851	0	3.462	0.764	0.934	0.053	0.011	2.813	dacite
28	5LA1416	1.554	1.034	20.773	65.935	292	2.391	0.595	0.832	0.031	0.036	6.474	dacite
29	5LA1416	1.693	0.923	20.783	68.133	0	2.581	0.387	0.896	0.061	0.01	4.271	dacite
30	5LA1416	1.058	0.961	23.765	65.659	174	2.462	0.765	1.064	0.083	0.009	3.906	dacite
AGV-1		3.866	0.325	16.551	62.614	0	3.089	5.171	1.048	0.046	0.102	6.895	standard
AGV-1		3.861	0.746	16.764	62.159	0	3.053	5.153	1.021	0.069	0.091	6.813	standard

		Ni	Cu	Zn	Ga	Rb	Sr	Y	Zr	Nb	Ba	Pb	Th
		ppm	ppm	ppm	ppm	ppm	ppm	ppm	ppm	ppm	ppm	ppm	ppm
1	5LA1211	24	78	146	28	68	247	51	139	32	1101	19	22
2	5LA1211	28	30	172	23	129	299	37	201	13	1024	91	17
3	5LA1211	27	36	122	31	81	358	27	136	20	1374	19	19
4	5LA1211	26	63	64	31	105	308	34	119	26	1184	38	29
5	5LA1211	27	48	304	26	137	267	34	157	25	1623	25	19
6	5LA1211	20	30	82	25	134	355	24	167	22	1616	37	27
7	5LA1211	27	36	91	33	120	387	37	124	23	1763	23	12
8	5LA1211	27	41	119	26	132	304	35	188	24	1423	37	18
9	5LA1211	20	27	85	28	84	250	30	132	17	1045	14	16
10	5LA1211	36	44	121	33	95	337	33	119	29	1763	29	21
11	5LA1211	21	52	84	28	76	244	35	184	22	923	31	36
12	5LA1211	22	38	69	24	66	223	30	256	22	1353	21	25
13	5LA1211	27	33	131	30	95	285	35	122	25	1473	24	12
14	5LA1211	31	31	218	32	97	307	36	116	29	1468	39	27
15	5LA1211	29	56	106	32	113	281	36	142	25	1503	30	25
16	5LA1416	30	20	122	31	99	331	37	144	28	1533	26	17
17	5LA1416	28	25	184	32	99	309	45	133	29	1309	32	24
18	5LA1416	16	8	20	9	0	32	27	567	26	90	7	13
19	5LA1416	21	51	66	24	92	391	28	198	13	1137	15	16
20	5LA1416	18	28	54	20	63	354	24	186	10	1036	14	4
21	5LA1416	36	11	60	18	74	434	20	149	41	2296	14	9
22	5LA1416	19	53	81	29	86	346	29	123	17	1342	25	20
23	5LA1416	28	24	109	29	75	278	36	133	20	1066	23	28
24	5LA1416	25	43	124	30	77	253	26	132	29	1081	21	22
25	5LA1416	24	90	87	35	113	374	41	139	19	1379	32	37
26	5LA1416	20	38	74	20	88	390	29	209	15	1249	16	4
27	5LA1416	17	22	50	21	116	225	28	279	23	1466	24	25
28	5LA1416	21	46	140	21	85	339	28	187	15	1579	15	11
29	5LA1416	17	51	41	24	100	398	23	193	13	1527	16	21
30	5LA1416	22	45	171	31	106	311	28	157	23	1143	35	24
AGV-1	standard	20	53	83	21	65	644	18	222	12	1179	27	4
AGV-1	standard	22	58	92	20	71	625	23	219	15	1068	22	4

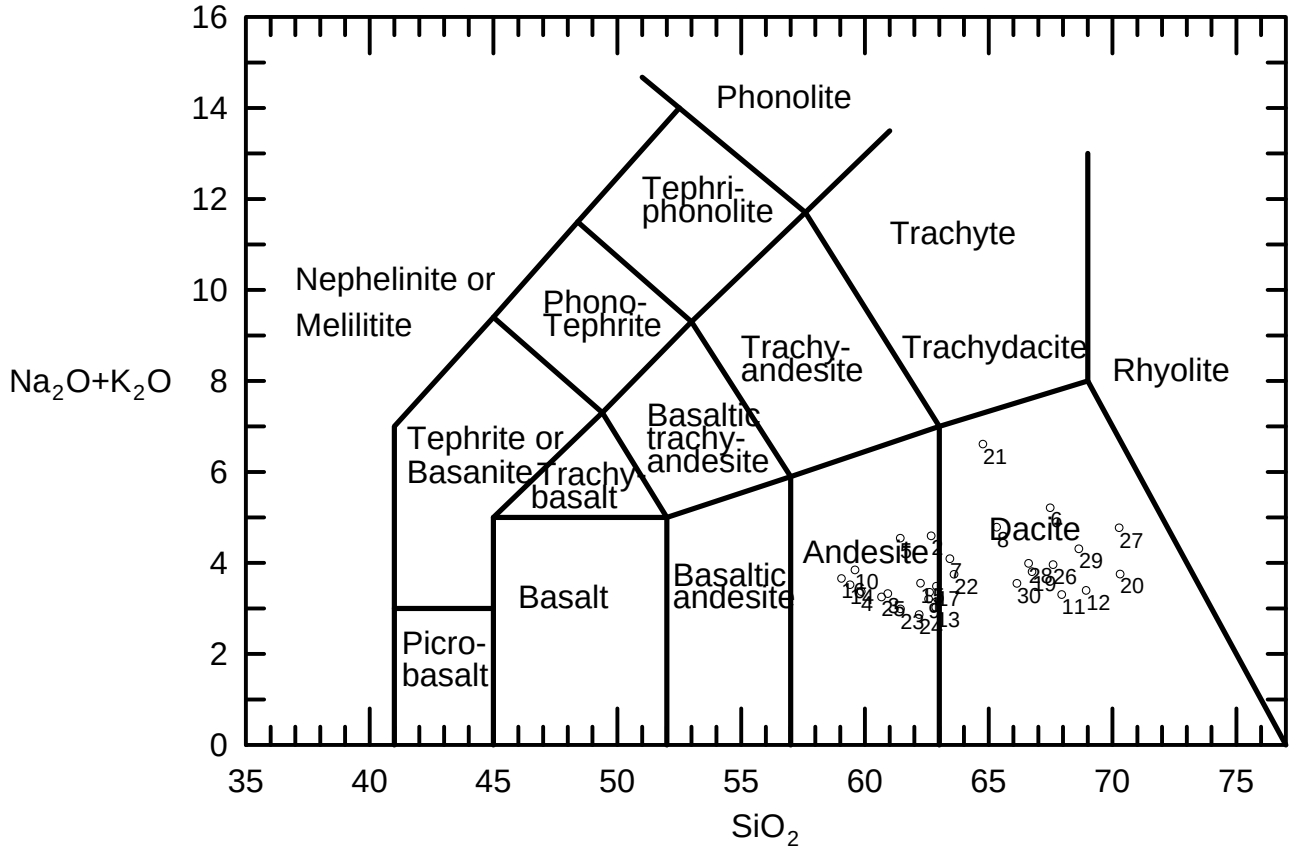

Figure 1. TAS plot of the archaeological specimens (Le Maitre et al. 1989).

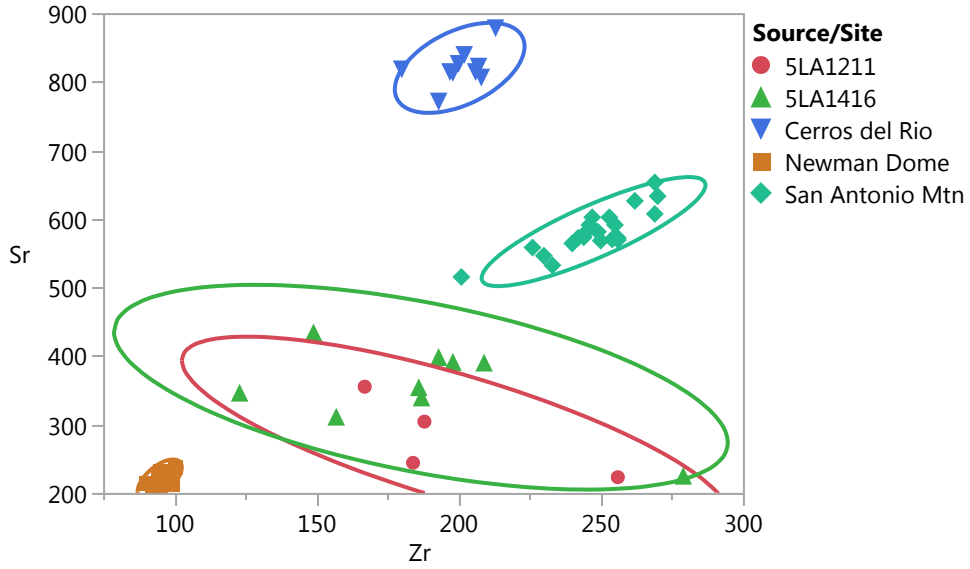

Figure 2. Zr versus Sr bivariate plot of northern New Mexico dacite sources and the archaeological artifacts (see Shackley 2011a). Confidence ellipses are at 95%.